NJC

ROYAL SOCIETY OF CHEMISTRY

PAPER

View Article Online
View Journal

Check for updates

Cite this: DOI: 10.1039/d0nj05845a

Published on 26 April 2021. Downloaded by Goa University on 5/3/2021 8:22:12 AM.

Characteristics of the pH-regulated aggregation-induced enhanced emission (AIEE) and nanostructure orchestrate *via* self-assembly of naphthalenediimide–tartaric acid bola-amphiphile: role in cellular uptake†

Sopan M. Wagalgave,[ab] Mahmood D. Aljabri,[c] Keerti Bhamidipati,[bd] Deepak A. Shejule,[a] Dinesh N. Nadimetla,[d] Mohammad Al Kobaisi,[c] Nagaprasad Puvvada,[bd] Sidhanath V. Bhosale *[ab] and Sheshanath V. Bhosale*[e]

In this study, tartaric acid (TA)-appended naphthalene diimide (NDI)-based bolaamphiphile (**NDI–TA**) was designed and synthesized to investigate the effect of the head group on the nanostructures fabricated by their self-assembly. Scanning electron microscopy (SEM) revealed the effect of the pH of the bolaamphiphile solution on the formation and morphology of the produced supramolecular nanostructures. It is known that the protonation/deprotonation of the TA head group in **NDI–TA** bolaamphiphile plays a significant role in compound nanostructures. Here, the circular dichroism (CD) study has revealed the presence of chirality at the supramolecular level of this nanostructure orchestrate. These findings show that the chirality of **NDI–TA** is significantly impacted in the pH range of 2 to 9. Importantly, the **NDI–TA** bolaamphiphile showed remarkable selectivity and biocompatibility in binding to markers in MDA-MB 231 cancer cells compared to NDI alone, even with its improved solubility. The cell morphology and uptake studies using confocal fluorescence microscopy exhibited blue to green fluorescence, a parameter that can be further explored for the efficient monitoring of intercellular pH levels and related cellular changes. Thus, our studies have demonstrated the potential of **NDI–TA** bolaamphiphile as a delivery agent for therapeutic intervention, and as an indicator of intercellular pH changes by binding to cell markers.

Received 1st December 2020,
Accepted 5th April 2021

DOI: 10.1039/d0nj05845a

rsc.li/njc

Introduction

The self-assembly of bolaamphiphile (bola) offers a reliable path to create a wide variety of nanostructures with specific functions.[1–3] Supramolecular non-covalent interactions such as π–π interactions, hydrogen bonding, electrostatic, and van der Waals forces are found in natural systems, and are considered important in the molecular design and fabrication of supramolecular architectures.[4–8] The nanostructure's morphology, tunability, intrinsic dynamics, and stimuli responsiveness are controlled by the precise molecular design of these organic building blocks.[9] In recent years, the design and synthesis of advanced building blocks for the fabrication of supramolecular soft materials that are responsive to external stimuli in assembly conditions has received significant attention.[10–13] To achieve a more complex and dynamic supramolecular nanoarchitecture of bolaamphiphile, various stimuli-responsive functionalities are controlled by variables (such as pH) as the chemical stimuli, and are responsible for the emission color, fluorescence brightness and shape observed. Light and temperature are both physical stimuli. Light is a good stimulus for photosensitizers and light harvesting film, and the temperature is reponsible for crystallization, clusteroluminescent AIE, among other processes.[13] Guided by chemical interactions, they have shown a successful approach to five mono[14–18] or multi-stimuli responsive[19–21] systems. Bolaamphiphile has attracted the attention of researchers,

[a] *Polymers and Functional Materials Division CSIR-Indian Institute of Chemical Technology, Hyderabad 500007, Telangana, India. E-mail: bhosale@iict.res.in*
[b] *Academy of Scientific and Innovative Research (AcSIR), Ghaziabad-201002, India*
[c] *School of Science, RMIT University, GPO Box 2476, Melbourne, Victoria, 3001, Australia*
[d] *Applied Biology Division CSIR-Indian Institute of Chemical Technology, Hyderabad 500007, Telangana, India*
[e] *School of Chemical Sciences, Goa University, Taleigao Plateau, Goa-403206, India. E-mail: svbhosale@unigoa.ac.in*

† Electronic supplementary information (ESI) available: Ft-IR, ^{1}H NMR, ^{13}C NMR, mass and HRMS of all newly synthesized compounds and theoretical calculations, UV-vis, DOS and CD, DLS and XRD. See DOI: 10.1039/d0nj05845a

Published on 26 April 2021. Downloaded by Goa University on 5/3/2021 8:22:12 AM.

owing to its molecular architecture diversity and application in various fields, such as medicine, biology, materials, and gene delivery.[22–25] To direct the self-assembled nanoarchitectures of bolaamphiphile, π-conjugated molecular building blocks with appropriate head groups are used.[26–32] Our previous works employed the naphthalenediimide (NDI) chromophore with a variety of head groups to fabricate different nanostructures *via* self-assembly in aqueous, as well as organic solvent systems.[33–41] Banerjee *et al.* previously reported NDI-based bolaamphiphiles, and they observed AIEE depending on the H^+ ion concentration of the medium. They discussed the write–erase–rewrite concept on the basis of the acidic medium.[38] It has been reported that the introduction of tartaric acid and other small organic head groups leads to the formation of a variety of supramolecular self-assembled structures.[42–44] Recently, our lab functionalized a NDI-conjugated core with lithocholic acid, which resulted in the self-assembled nanostructure formation inside the cell exhibiting blue fluorescence when observed under a confocal microscope.[45]

Thus, NDI and its derivatives with their self-assembled nanostructures demonstrated their potential in binding to cell markers, cell fluorescence imaging and drug delivery agents.[46–48,49*a*]

In the present study, we designed and synthesized NDI bolaamphiphile with tartaric acid head groups. The –COOH end group of tartaric acid can be either protonated or deprotonated with a change in the pH in aqueous environment. This will largely lead to a change in the intermolecular H-bonding and ionic interactions of the bolaamphiphiles. Such a change in the molecular structure at different pH values resulted in the formation of diverse morphologies, such as cubic, truncated cubic, and fractal grass-like structures in water. The present work utilizes H-bonding, electrostatic interactions, amide-hydrogen bonding, and π–π interactions to produce various morphologies from the **NDI–TA** building block. Finally, we utilized these self-assembled **NDI–TA** functionalized nanostructures with their improved solubility to study its biocompatibility and demonstrate its efficient cellular uptake in cancer cells.

Experimental details

Materials and methods

All the chemicals and solvents, such as naphthalene-1,4,5,8-tetracarboxylic anhydride (NDA), di-*tert*-butyl dicarbonate, di-*o*-acetyl-L-tartaric anhydride, triethylamine, ethylenediamine, and isopropanol, were purchased from TCI, Chennai, Tamil Nadu, and Sigma-Aldrich, Bengaluru, Karnataka, India. Cytotoxicity assays were recorded on a VARIOSKAN multi-mode microplate reader (Thermo Fisher Scientific). Confocal images were recorded on an Olympus FLUOVIEW FV10i confocal microscope. Cell culture materials were procured from Gibco, USA and Hi-media, India. 3-(4,5-Dimethylthiazol-2-yl)-2,5-diphenyltetrazolium bromide (MTT), fluoro-shield mounting medium, and 4% formaldehyde solution were purchased from Sigma Aldrich.

^{1}H-NMR were recorded on Bruker Avance-400 MHz and 500 MHz spectrometers at room temperature. ^{13}C NMR spectra were recorded at 100 MHz and 125 MHz, and tetramethylsilane (TMS) was used as the internal standard. FT-IR measurements were recorded on a Thermo Nicolet Nexus 670 FT-IR spectrometer. UV-Vis absorption spectra were measured on the Shimadzu UV-1800 spectrophotometer. Fluorescence spectra were recorded using a Shimadzu RF-6000 spectrofluorophotometer.

Synthesis of di-*tert*-butyl((1,3,6,8-tetraoxo-1,3,6,8 -tetrahydrobenzo [*lmn*][3,8] phenanthroline-2,7-diyl)bis(ethane-2,1-diyl))dicarbamate (3)

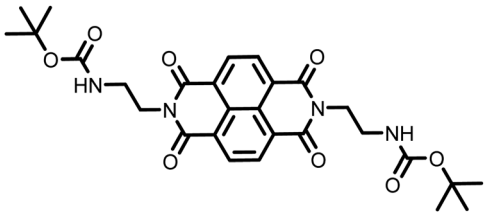

Mono boc-ethylene diamine **2** (3.35 g, 20.29 mmol) and Et_3N (5.65 mL, 40.58 mmol) were added to a mechanically stirred suspension with **NDA-1** (2.5 g, 9.22 mmol) in iPrOH (60 mL). The resulting mixture was refluxed for 72 h under N_2 atm. After cooling at room temperature, a white solid was obtained, which was filtered and washed with MeOH. Then, the reaction mixture was subjected for purification using column chromatography (60–120 mesh; SiO_2) as a stationary phase and CH_2Cl_2 : MeOH (98 : 2) as an eluent to yield **3** as a solid (3.5 g, yield: 68%). FT-IR (KBr, cm^{-1}): ν 3357.19 (NH-stretching band), 3065.92–2982.73 (–CH stretching), 1690.56 (imide carbonyl symmetric stretching), 1659.07 (imide carbonyl asymmetric stretching), 1532.19, 1350.27, 1178.56, 770.76; ^{1}H NMR (400 MHz, $CDCl_3$): δ 8.75 (s, 4H), 4.91 (br, s, 2H), 4.39–4.36 (m, 4H), 3.57–3.56 (m, 4H), 1.22 (s, 18H); ^{13}C NMR (75 MHz, $CDCl_3$ + DMSO-d_6): δ 167.82, 161.10, 135.45, 131.44, 131.36, 83.42, 82.67, 45.51, 43.40, 32.99.

Synthesis of 2,2′-(1,3,6,8-tetraoxo-1,3,6,8-tetrahydrobenzo [*lmn*][3,8]phenanthroline-2,7-diyl)bis(ethan-1-aminium) (4)

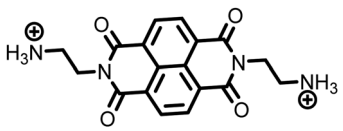

Trifluoroacetic acid (5 mL) was added dropwise to a stirred suspension of compound **3** (1 g, 1.8 mmol) in CH_2Cl_2 (10 mL) at 0 °C. The resulting brown solution was stirred for 3 h at rt. The solvent was removed under reduced pressure by a rotary evaporator. The residue was treated with *n*-hexane (3 × 50 mL) to remove an excess of TFA under reduced pressure to afford a white solid of compound **2**, 0.63 g (yield: 95%). The obtained compound **4** was used in the next step. FT-IR (KBr, cm^{-1}): ν 3447.64 (–NH stretching with hydrogen bonding), 3070.53–2951.93 (–CH stretching), 1676.97 (imide carbonyl stretching), 1340.77, 1157.41, 771.31; ^{1}H NMR (300 MHz, DMSO-d_6): δ 8.72 (s, 4H), 7.99 (br, s, 6H), 4.38–4.34 (m, 4H), 3.22–3.20 (m, 4H); ^{13}C NMR (75 MHz, DMSO-d_6): δ 163.22, 158.41, 157.97, 130.35, 126.53, 126.20, 37.88, 37.43.

 This journal is © The Royal Society of Chemistry and the Centre National de la Recherche Scientifique 2021

Published on 26 April 2021. Downloaded by Goa University on 5/3/2021 8:22:12 AM.

Synthesis of 2,3-diacetoxy-4-((2-(7-octyl-1,3,6,8-tetraoxo-3,6,7,8-tetrahydrobenzo[*lmn*][3,8] phenanthrolin-2(1*H*)-yl)ethyl)amino)-4-oxobutanoic acid (NDI–TA)

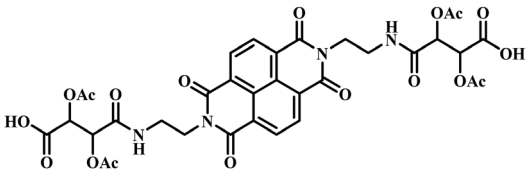

Naphthalene diimide bolaamphiphile **4** (23 mmol) was treated with di-*o*-acetyl-L-tartaric anhydride **5** (50 mmol) in DMF (20 mL) at room temperature for 24 h under nitrogen atmosphere. The reaction mixture was monitored by TLC. After completion of the reaction, the excess solvents were removed under reduced pressure. The crude product was washed with pentane followed by DCM. The product appeared as a white solid as **NDI–TA**, yield 64%. FT-IR (ν, cm^{-1}): ν 3421.34–3245.07 (–NH and –OH stretching with hydrogen bonding), 2948.75 (–CH stretching), 1744.07 (ester carbonyl stretching), 1702.46 (acid carbonyl stretching), 1678.51 (imide carbonyl stretching), 1542.88, 1371.38, 1211.38, 1068.07, 767.05; ^{1}H NMR (500 MHz, $CDCl_3$ + TFA) δ 8.81 (s, 4H), 7.63–7.61 (t, J = 5.64 Hz, 2H), 5.75–5.75 (d, J = 2.44 Hz, 2H), 5.64–5.64 (d, J = 2.59 Hz, 2H), 4.52–4.50 (t, J = 5.95 Hz, 4H), 3.96–3.89 (m, 2H), 3.76–3.70 (m, 2H), 2.34 (s, 6H), 2.23 (s, 6H); ^{13}C NMR (100 MHz, $CDCl_3$ + TFA) δ 172.71, 171.52, 168.11, 164.19, 131.99, 126.77, 126.23, 71.44, 70.96, 39.76, 39.47, 20.11, 19.95; ESI-Mass m/z $[M + H]^+$ 785; HRMS: calculated for chemical formula: $C_{34}H_{33}O_{18}N_4$ $[M + H]^+$ m/z 785.17844, found: 785.17768; HPLC: purity of **NDI–TA** is 97.8%, 0.1% formic acid in acetonitrile (see ESI,† Fig. S12).

High-performance liquid chromatography (HPLC). HPLC analysis was carried out with Shimadzu Lab Solutions at room temperature, flow rate: 1 mL min^{-1}, retention time: 4.036 min (major), 2.794 min (minor).

Phosphate buffer. $Na_2HPO_4{\cdot}7H_2O$ (2.021 g) and $NaH_2PO_4{\cdot}H_2O$ (0.339 g) in 80 mL with 7.4 pH and 0.1 M solution.

UV-Vis spectroscopy. The UV-Vis absorption spectra were recorded in a UV 1800 Shimadzu spectrophotometer at room temperature. UV-Vis spectra of **NDI–TA** were recorded in phosphate buffer with various pH values ranging from 2.0–9.0 with the quartz cell path length of 1.0 cm.

Fluorescence spectroscopy. The fluorescence emission spectra were recorded on a RF-6000 Shimadzu Fluorescence Spectrophotometer. The emission spectra of **NDI–TA** were recorded in phosphate buffer at room temperature with the pH value adjusted between 2 and 9 in the quartz cell upon excitation at λ_{ex} = 370 nm.

Fluorescence lifetime measurements. The time-resolved spectroscopy measurements were carried out on a picosecond time-correlated single photon counting (TCSPC) system (FluoroLog3-Triple Illuminator, IBH Horiba JobinYvon) using a picosecond light emitting diode laser (NanoLED, λ_{ex} = 370 nm). The samples for the analyses were prepared in phosphate buffer solution evaluated using a 1 cm cuvette at 25 °C.

Circular dichroism. CD spectra were examined on an AVIV 202 CD spectrometer under a nitrogen atmosphere. The experiments were carried out in a quartz cuvette (Hellma) with a 1 mm path length over the range of 330–430 nm in phosphate buffer solution.

Scanning electron microscopy (SEM). Images were recorded on an FEI Nova NanoSEM (Hillsboro, USA) operating at a high vacuum, which provided direct visualization of the self-assembled nanostructures. The samples were prepared as follows: first, the silicon wafers were washed by acetone, followed by ethanol and Milli-Q water, respectively. After the samples were placed on silicon wafers, the solvent was evaporated and then the air-dried sample was sputter-coated with gold for 10 s at a 0.016 mA Ar plasma (SPI, West Chester, USA).

X-Ray diffraction (XRD) measurements. XRD measurements were performed on a Bruker D8 FOCUS diffractometer using a Cu target radiation source (λ = 0.15418 nm).

Dynamic light scattering experiment. All DLS experiments were performed with a Malvern Instrument Zetasizer Nano Series (Malvern Instruments, Westborough, MA, USA). The DLS of **NDI–TA** (1×10^{-5} M) in buffer solution (3 mL) was measured at different pH values. The experimental temperature was maintained at 25 °C temperature.

Molecular modelling. Density functional theory (DFT) calculations with no consideration of dispersion interactions in a gas phase was conducted using the Gaussian 09 suite of programs at B3LYP/6-31G(d,p)//B3LYP/6-311G(d,p) level of theory.

Cell culture. Cancerous cells MDA-MB 231 (Human mammary gland adenocarcinoma cell line) and non-cancerous cells HEK 293 (Human embryonic kidney epithelial cells) were obtained from the National Centre for Cell Sciences (NCCS), Pune, India. The cells were cultured in DMEM (Dulbecco Modified Eagle Medium) media (Gibco) and RPMI-1640 (Roswell Park Memorial Institute) media (Hi-media) supplemented with 10% (v/v) fetal bovine serum, 1% L-glutamine, 1% NEAA, 1% penicillin, and 1% streptomycin. All cells were maintained in a humidified 5% CO_2 incubator at 37 °C.

Cytotoxicity studies using MTT assay. The cell cytotoxicity study of **NDI–TA** and NDI was carried out using MTT (3-(4,5-dimethylthiazole-2-yl)-2,5-diphenyltetrazolium bromide reagent) assay in MDA-MB 231 cancerous cells and HEK 293 normal cells seeded and grown in 96-well plates separately for 24 h at 1×10^4 cells per well in triplicate for 48 h at various concentrations (1, 2.5, 5, 10, 25 and 50 μg/100 μL).[50,53] The cells were then washed twice with 1× PBS, and further incubated with 450 μL (1 g mL^{-1}) of MTT solutions at 37 °C for 3–4 h. Then, the MTT solubilizing buffer was used to dissolve formazan crystals. The absorbance was calculated at 570 nm by using a Multimode microplate reader (Varioskan, Thermo Fisher Scientific).

Intracellular uptake study using confocal microscopy. The cellular uptake efficiency and the cytoplasmic distribution of **NDI–TA** and NDI were done in MDA-MB 231 cells (Human mammary gland

Published on 26 April 2021. Downloaded by Goa University on 5/3/2021 8:22:12 AM.

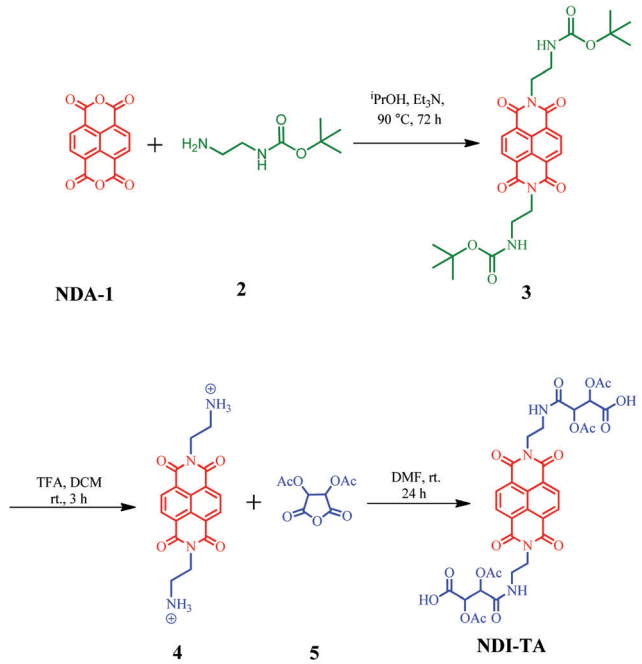

Scheme 1 Synthesis of the **NDI–TA** bolaamphiphile.

adenocarcinoma cell line). The cells were seeded (5×10^4) in 35 mm cover glass with 1 ml of growth medium and grown at 37 °C. The cells were then treated with **NDI–TA** and NDI at different time points of 3, 6, and 24 h with a concentration of (5 μg/100 μl). After that, the cells were washed with 1× PBS and fixed using 4% formaldehyde solution. The cells were then washed again with a 1× PBS solution twice to remove the excess formaldehyde solution, and mounted onto a microscopic slide using a Fluoro-shield mounting solution. The fluorescent images were then recorded using a confocal microscope (Olympus FLUOVIEW FV10i) at 60× magnification and 60× + 3× zoom magnification.

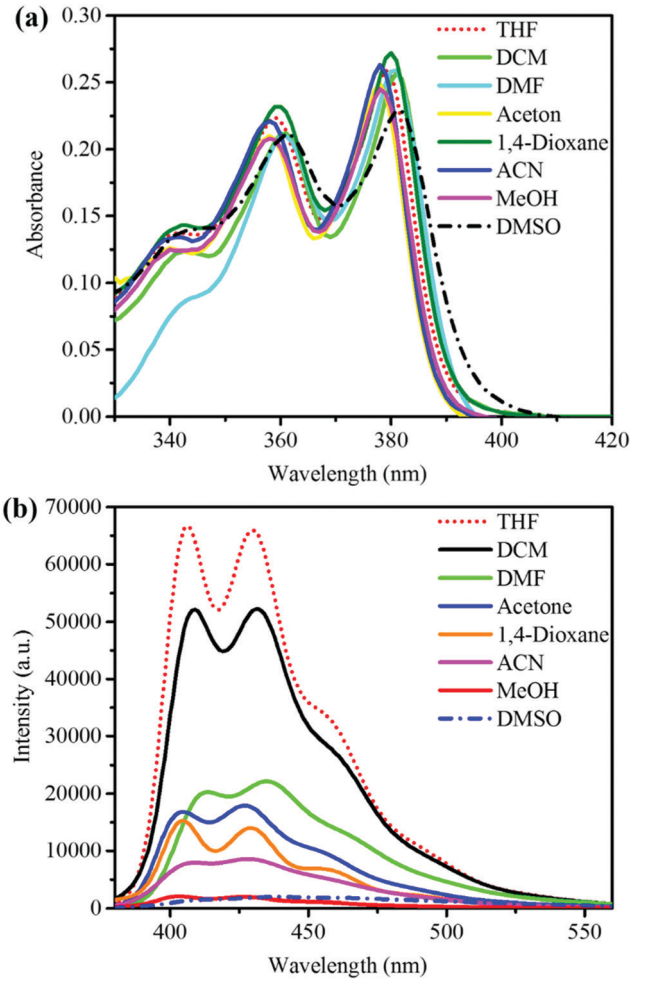

Fig. 1 (a) UV-vis absorption and (b) emission (excitation wavelength λ_{ex} = 370 nm) spectra of **NDI–TA** in various solvents.

Results and discussion

Synthesis

Synthesis of **NDI–TA** was achieved *via* a multistep reaction strategy starting from naphthalene dianhydride. At the first step, **NDA-1** (9.22 mmol) is reacted with mono-Boc-protected ethylenediamine **2** (20.29 mmol) in the presence of triethyl amine (40.58 mmol) in isopropanol to yield compound **3**. Subsequently, compound **3** (1.8 mmol) was subjected to the deprotection of the Boc protecting group in TFA/DCM at room temperature to give **4**. Furthermore, **4** (23 mmol) is reacted with 2,5-dioxotetrahydrofuran-3,4-diyl diacetate **5** (50 mmol) in DMF at room temperature to yield bolaamphiphile **NDI–TA**. **NDI–TA** is fully soluble in a DMSO : phosphate buffer solution (1 : 9) with a pH range of 2 to 9 to lead to the formation of aggregates (Scheme 1).

Spectroscopic properties

The effect of solvents on the optical properties of NDI–TA. UV-Vis absorption and emission spectroscopy techniques were used to elaborate both the properties optical and photophysical of **NDI–TA** in various solvents, including tetrahydrofuran (THF), dichloromethane (DCM), dimethylformamide (DMF), acetone, 1,4-dioxane, acetonitrile (ACN), methanol (MeOH) and dimethyl sulfoxide (DMSO) at room temperature (Fig. 1a and b). The UV-Vis absorption spectra of **NDI–TA** in DMSO, DCM and DMF show a bathochromic shift in the absorbance band at lower energy, which is attributed to the coordination of the solvent molecules with the acid head groups. Table 1 summarizes the UV-Vis data shown in Fig. 1a, indicating very small differences in the absorbance peaks corresponding to the differences in the nature of the solvents and the solvation coordination.

The emission spectra of **NDI–TA** are shown in Fig. 1b. Excitation of **NDI–TA** in THF exhibits strong fluorescence emission peaks at 404 nm and 429 nm, with the quantum yield (Φ) of 7.9. This indicates that **NDI–TA** in THF is in its monomeric form. As illustrated in Fig. 1b, in DCM (Φ = 6.7), the emission is found at the maximum. **NDI–TA** in organic solvents (such as DMF, acetone, 1,4-dioxane, and acetonitrile) is emissive. Whereas, **NDI–TA** is non-emissive in methanol and DMSO.

 This journal is © The Royal Society of Chemistry and the Centre National de la Recherche Scientifique 2021

Published on 26 April 2021. Downloaded by Goa University on 5/3/2021 8:22:12 AM.

Table 1 UV-Vis absorption and fluorescence of **NDI–TA** in different solvents

	Absorption (nm) Absorption coefficient (ε/M^{-1} cm^{-1})			Emission (nm)		
Solvent	Shoulder	Peak I	Peak II	Peak I	Peak II	Quantum yield (Φ)
1,4-Dioxane	341	359 (2.32×10^4)	379 (2.71×10^4)	404	429	1.3
DCM	340	361 (2.11×10^4)	381 (2.56×10^4)	408	431	6.7
THF	340	359 (2.24×10^4)	379 (2.58×10^4)	406	430	7.9
Acetone	340	357 (2.09×10^4)	378 (2.48×10^4)	404	426	1.7
ACN	339	357 (2.21×10^4)	377 (2.62×10^4)	406	428	1.0
MeOH	340	358 (2.07×10^4)	378 (2.44×10^4)	—	—	0.2
DMF	343	360 (2.10×10^4)	380 (2.59×10^4)	412	435	2.3
DMSO	341	361 (2.11×10^4)	381 (2.29×10^4)	—	—	0.1
pH-2	342	361 (4.67×10^4)	382 (5.69×10^4)	393	410	1.3@560 nm
pH-7	343	361 (4.21×10^4)	382 (5.15×10^4)	392	411	2.6@560 nm
pH-9	342	361 (4.52×10^4)	382 (5.42×10^4)	392	411	4.2@560 nm

Moreover, in methanol (Φ = 0.2) and DMSO (Φ = 0.1), the fluorescence intensity is completely diminished. The fluorescence quenching in DMSO > MeOH > ACN > 1,4-dioxane > acetone > DMF is attributed to the aggregation of **NDI–TA** in these solvents.

To explore the pH-dependent supramolecular assembly behaviour of the **NDI–TA** bolaamphiphile, UV-Vis absorption technique was employed. The pH dependent variation between 2 to 9 on 1×10^{-5} M solution of **NDI–TA** was studied using UV-Vis absorption spectroscopy (Fig. 2a and b). At pH 7, **NDI–TA** exhibits two well-resolved strong absorbance peaks at 360 and 382 nm, attributed to the π–π^* transition, and a shoulder peak at 347 nm. The shoulder peak is typical of the NDI core subunit. No significant change in the UV-Vis absorption peaks was detected by varying the pH value from 7 to 3 in phosphate buffer solution. As shown in Fig. 2a, **NDI–TA** displayed an increase in the intensity of the absorbance peak at pH 2. Furthermore, varying the pH of the **NDI–TA** solution from 7 to 9 gives a small increase in the absorbance intensity, indicative of the stacking of **NDI–TA** in the self-assembly formation due to deprotonation of the acid head group in basic conditions.

Furthermore, the self-assembly of the **NDI–TA** chromophore was investigated by pH-dependent fluorescence spectroscopy, as depicted in Fig. 3a and b. Upon excitation at 370 nm, **NDI–TA** at pH 7 exhibits strong two emission peaks at 390 and 420 nm, along with two unexpected small peaks at 550 and 590 nm (Φ_{560} = 2.6), suggesting the chromophore undergoes aggregation. The fluorescence quantum yield was calculated by using Rhodamine B as the standard substance.[49b] The peaks at 390 and 420 nm slightly decreased by changing pH from 7 to 6,

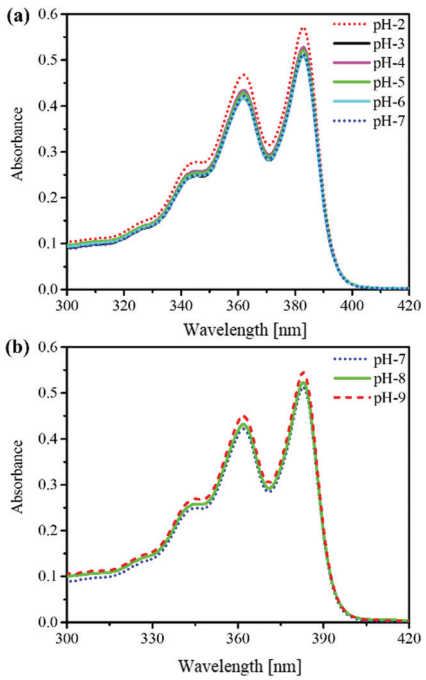

Fig. 2 UV-vis absorption spectra of **NDI–TA** (1.0×10^{-5} M) in phosphate buffer at (a) pH 7 to 2, and (b) pH 7 to 9 at room temperature.

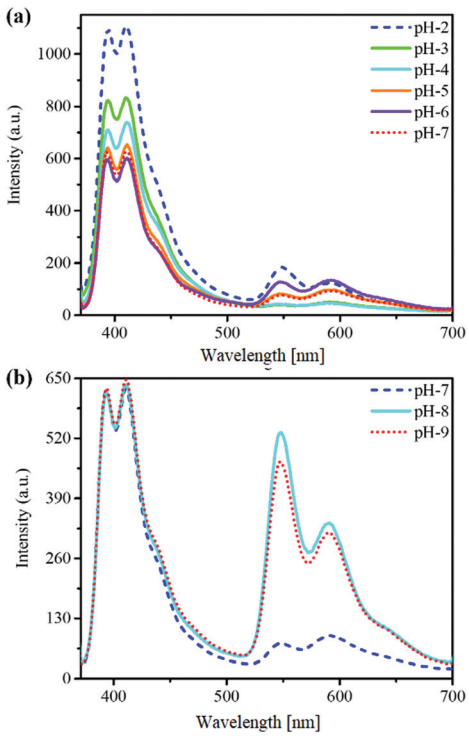

Fig. 3 Fluorescence spectra of **NDI–TA** (1.0×10^{-5} M) upon excitation at = 370 nm in phosphate buffer by changing the pH value from (a) 7 to 2 and (b) 7 to 9 at 25 °C.

Published on 26 April 2021. Downloaded by Goa University on 5/3/2021 8:22:12 AM.

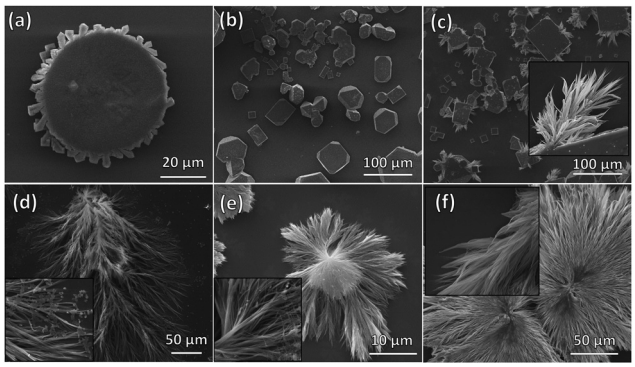

Fig. 4 SEM micrographs of **NDI–TA** (1×10^{-5} M) deposited from solutions at pH (a) 3, (b) 4, (c) 5, (d) 6, (e) 7, and (f) 8.

whereas the peaks at 550 and 590 nm increased, indicating the aggregation of **NDI–TA**. Furthermore, the change in pH from 6 to 2 displays an increase in the emission intensity peaks at 390, 420, 550 and 590 nm significantly, indicating that **NDI–TA** undergoes aggregation-induced enhanced emission (AIEE). Thus, a change in the pH value from 7 to 2 with Φ at 560 = 1.3 triggers the monomeric **NDI–TA** to self-assemble into an aggregation state, and induces the AIEE characteristics. Furthermore, in basic conditions, **NDI–TA** at pH 8 and 9 shows strong emission peak enhancement at 550 and 590 nm (Φ_{560} = 4.2). As compared to the acidic condition, this indicates that **NDI–TA** exhibits strong AIEE characteristics in basic media due to the increasing π–π* transition of the NDI molecules with observed J-type aggregation in pH 8 and 9, and decreasing the H^+ concentration increasing the fluorescence.[38a] Interestingly, **NDI–TA** displayed AIE properties in water at higher pH, such as 8 and 9, compared to that in the organic solvent.[38b] We presume that in the organic solvent, the H-bonding is stronger than in water. This may lead to a different aggregation state, such as ACQ and AIE, respectively.

Lifetime measurements

Time-resolved fluorescence lifetime measurements were carried out in the nanosecond scale of the **NDI–TA** bolaamphiphile molecule (see ESI,† Fig. S13) with different emission wavelengths in alternative pH values, using time-correlated single photon counting (TCSPC). TCSPC studies of **NDI–TA** were carried out in phosphate buffer solution at pH-3, pH-7 and pH-9 at 370 nm emission excitation. The lifetime measurements at pH-3, pH-7 and pH-9 exhibited a decay lifetime of two component systems. The first components are 0.569 ns (52.69%), 4.305 ns (4.71%) and 4.063 ns (4.87%) decay. The component are 5.171 ns (47.31%), 0.030 ns (95.29%) and 0.034 (95.13%), respectively (Table S1, ESI†). We assume the quenching of the fluorescence decay is due to the self-assembly and aggregation of **NDI–TA**, while increasing the pH increases the lifetime in the first components and decreases in the second components. These components are but different particles of aggregation.[50]

Morphology study

The microstructures of **NDI–TA** were studied using scanning electron microscopy (SEM) (Fig. 4). Solids were deposited on a silicon wafer by solvent evaporation from solutions at various pH values ranging from 2 to 9. Cubic highly crystalline microstructures resulted at low pHs, where the **NDI–TA** carboxylic groups were fully protonated. Increasing the pH increased the size of the cubic entities up to pH 5, where the observed microstructures became a mix of cubic or truncated cubic structures and fractal grass-like microstructures. The fractal structure becomes the only feature in basic conditions, where various ionic species of **NDI–TA** are present. The domain of the fractal features and the size of its subunits grow larger with increasing basic conditions. The features observed in the SEM micrographs can be described by two

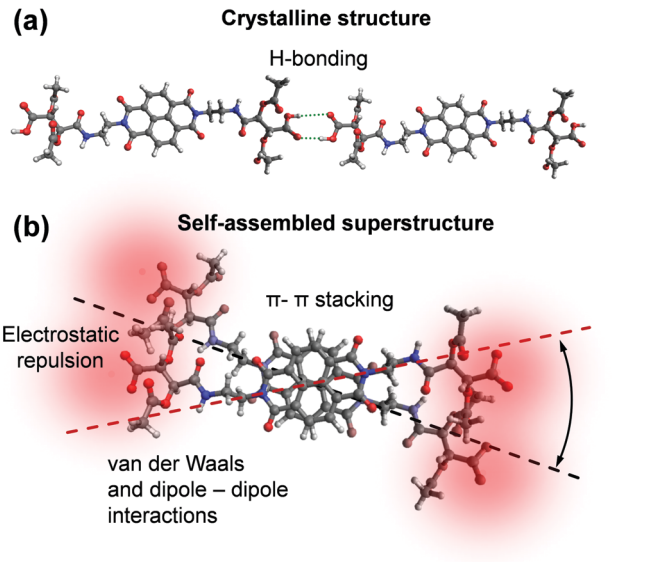

Fig. 5 Schematic self-assembly of the **NDI–TA** molecules at fully protonated (a) and fully deprotonated carboxylic groups (b) in highly acidic and highly basic conditions, respectively.

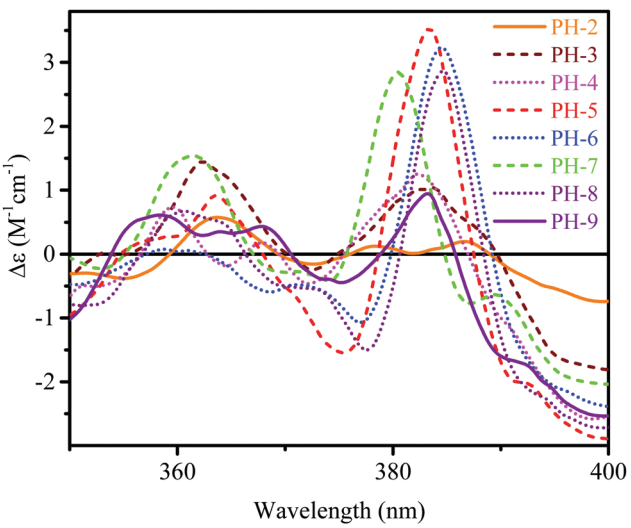

Fig. 6 CD spectra of **NDI–TA** at 1×10^{-5} M by changing the pH from 2 and 9, recorded at 25 °C.

 This journal is © The Royal Society of Chemistry and the Centre National de la Recherche Scientifique 2021

Published on 26 April 2021. Downloaded by Goa University on 5/3/2021 8:22:12 AM.

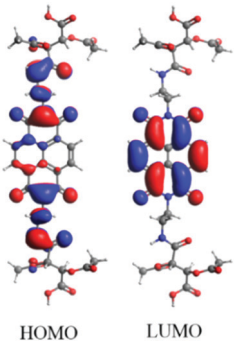

Fig. 7 The frontier molecular orbital (HOMO and LUMO) wave functions of **NDI–TA** as calculated using TDDFT at the B3LYP/6-311+G(d,p) level of theory.

modes of crystallization/self-assembly. The first is of the fully protonated **NDI–TA** molecule and dominated by hydrogen bonding between the carboxylic acid and amide groups, and the π–π and hydrophobic interactions of NDI and acetyl moieties. The second is of the deprotonated species of the **NDI–TA** molecule in basic conditions giving the fractal structure with grass-like with 2D subunit structure. Here, the self-assembly preferentially occurs in the directions where the hydrophobic interactions are dominant and the ionic moieties are ether well-solvated in the aqueous environment or positioned far enough due to electrostatic repulsion.

Thus, at neutral pH, the peripheral carboxylic acid head groups undergo strong hydrogen bonding with H_2O. Under acidic conditions, the –COOH groups undergo molecular dimerization. Upon increasing the pH to basic conditions (pH $>$ 7), a solution of **NDI–TA** formed different types of stacking, with the deprotonated head group at the outer surface.

Dynamic light scattering (DLS) study

The self-assembled nanomaterials with size distribution were investigated in **NDI–TA** solutions at pH values between 2 and 9, employing dynamic light scattering (DLS) measurements, and are illustrated in Fig. S14 (ESI†). The self-assembled materials of **NDI–TA** (1×10^{-5} M) at acidic pH values of 2, 3, 4, 5, and 6 give peaks at 810, 533, 513, 800, and 597 nm hydrodynamic diameter aggregates, respectively. The **NDI–TA** solution at pH 7, 8, and 9 produced aggregates with 759, 515, and 834 nm hydrodynamic diameter, respectively. The relatively large microstructures, observed in acidic, neutral and basic solutions, indicate that **NDI–TA** tends to self-assemble in an aqueous environment due to hydrophobic π–π and van der Waals solvophobic interactions. This is despite the carboxylic functionality, which makes the molecule relatively soluble in water. DLS measurements support the results obtained from SEM (Fig. 4), where we find the crystalline and grass-like fractal morphology with subunits in similar dimensions.

XRD investigation

Powder XRD of **NDI–TA** prepared from solutions at various acidic and basic pH values is depicted in Fig. S15 (ESI†). The powder gives a highly crystalline pattern at pH 2 and 3 with the main peaks at a different angle, showing a pH-dependent crystal growth. The strong crystalline nature of the material is significantly reduced when the pH is shifted to the neutral and basic environment. This is in agreement with the SEM results that showed a similar trend in the microstructure evolution with the change of pH.

Mechanism for self-assembly

The various ionic species of **NDI–TA** and its non-ionic form, which exist in basic and acidic solutions, respectively, aggregate to form microstructures *via* two pathways. In highly acidic solutions, the carboxylic functionalities are protonated and available to form double H-bonds at both ends. In addition to this, hydrophobic and van der Waals interactions can affect the

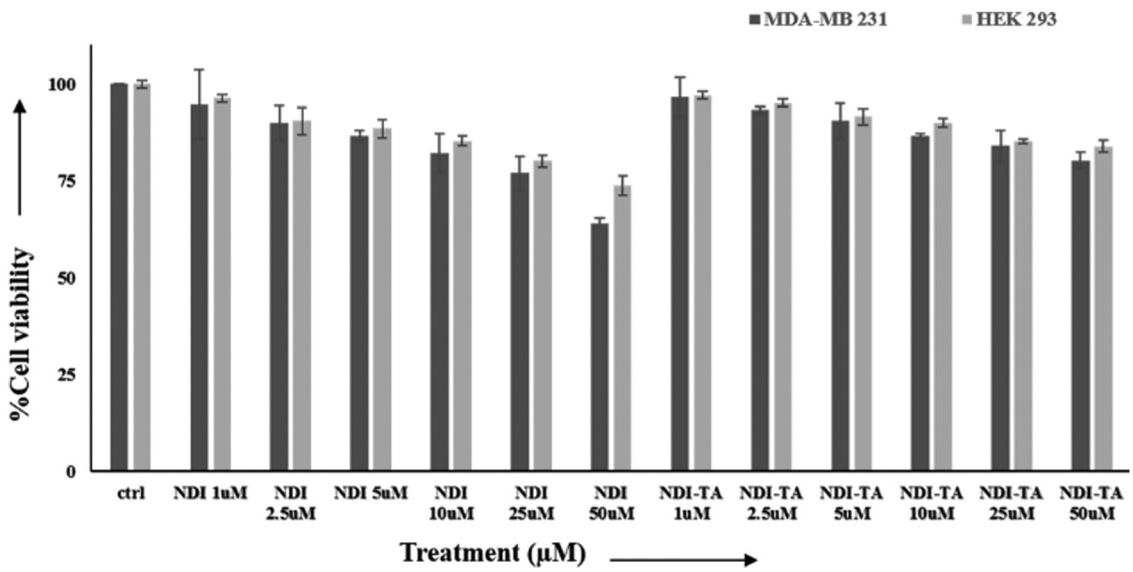

Fig. 8 **NDI–TA** & NDI comparative cell viability analysis on MDA-MB 231 (cancer cells) and non-HEK 293 (non-cancer cells) at various concentrations (48 h).

Published on 26 April 2021. Downloaded by Goa University on 5/3/2021 8:22:12 AM.

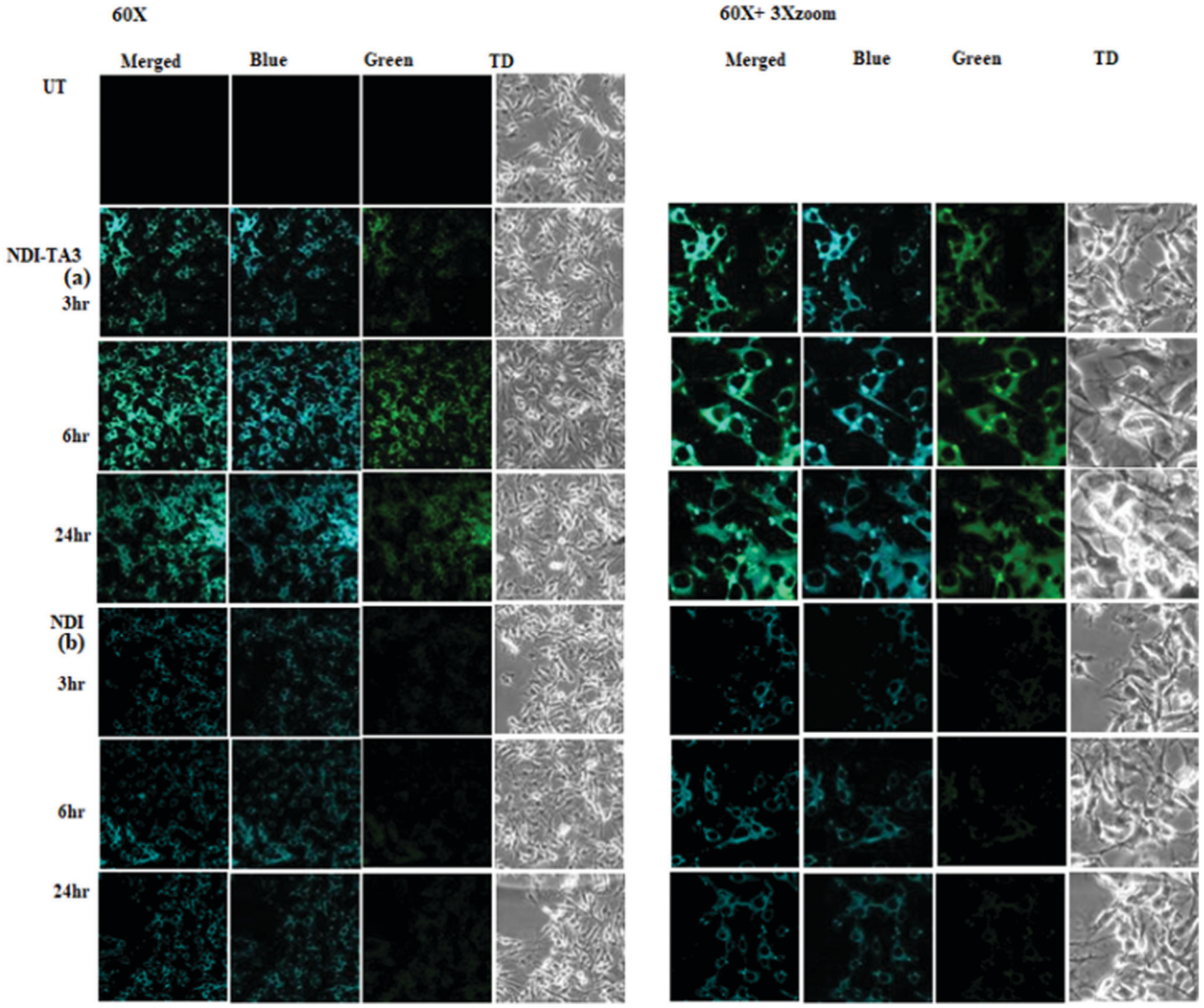

Fig. 9 Confocal images of fixed MDA-MB 231 human adenocarcinoma cells after treatment of (a) **NDI–TA**, (b) NDI at 3 h, 6 h and 24 h time points. 60× magnification with 10 μm scale.

self-assembling geometry, while the large TA moieties minimise the interactions between the amide groups. This results in a crystalline microstructure, as can be seen in the SEM micrographs in Fig. 4a and b and presented schematically in Fig. 5a. At highly basic conditions, the carboxylic functional groups are mainly deprotonated and carry a negative charge. This induces electrostatic repulsion at both **NDI–TA** molecule ends during self-assembly, creating an evolving twist that breaks the crystalline symmetry and produces a grass-like fractal structure, as can be seen in the Fig. 4e and f SEM micrographs and Fig. 5b scheme. Although the twist is introduced *via* electrostatic interaction, the hydrophobic π–π and van der Waals interactions are the major forces governing the self-assembly in the aqueous solution. In the medium range of pH values, a mixture of the crystalline and grass-like structure is produced (Fig. 4c and d).

Circular dichroism characteristics

The circular dichroism (CD) spectroscopy technique is an important technique due to its sensitivity to the chirality of the molecular architecture in its monomeric and self-assembled states. As illustrated in Fig. 6, at pH 7, **NDI–TA** exhibits the Cotton effect with two strong +ve peaks at 360 and 380 nm and −ve Cotton effect at 370 nm, indicating a chiral superstructure of **NDI–TA** aggregates. Decreasing the pH to 6, a comparable Cotton effect was observed with a change in the peak intensity and position. At pH 6, the +ve Cotton effect peak at 360 significantly decreased and the −ve peak at 370 nm increased in intensity, and shifted to 385 nm. Further decreasing the pH to 5 shows three strong CD signals at 360 (+ve), 275 (−ve), and 385 nm (+ve). At pH 4 and 3, a broad peak at 382 nm (+ve) with shoulders appeared. However, at pH 2, the peak intensity was negligible at 385 nm. Moreover, at basic pH of 8 and 9, a broad +ve peak at 360 nm, −ve peak at 375 nm and +ve peak at 385 nm can be observed. Thus, the CD results suggest a similar trend in conformation change with a change in the pH from 7 to 2 and from 7 to 9. From these results, we conclude that the **NDI–TA** molecular architecture, as well as its self-assembled material, are chirally active.

 This journal is © The Royal Society of Chemistry and the Centre National de la Recherche Scientifique 2021

Published on 26 April 2021. Downloaded by Goa University on 5/3/2021 8:22:12 AM.

Computational calculations

The time-dependent density functional theory (TDDFT) calculations *in vacuo* were conducted using the Gaussian 16 suit of programs[51] at the B3LYP/6-31G(d,p)//B3LYP/6-311G(d,p) level of theory. The Gauss-Sum 3.0 program[52] was used to calculate the contributions to the HOMO and LUMO orbitals to give a density of states (DOS) spectra produced by convoluting the HOMO and LUMO orbitals information obtained from the Gaussian modelling results. The TDDFT calculation of **NDI–TA** gave a HOMO (−7.60 eV)–LUMO (−4.12 eV) gap of 3.48 eV, while the major contribution of the HOMO → LUMO transition is at 389.0 nm (see ESI,† Table S2). The molecular orbital electron density was determined with *N*-substitutions and the NDI core, respectively, making the NDI core the acceptor part of the molecule in a HOMO–LUMO donor–acceptor electron transfer (see Fig. 7 and ESI,† Fig. S16).

The simulated CD spectrum of **NDI–TA** in the gas phase shows a similar pattern to the molecule in neutral pH solution. This is indicative of the observed chirality in the measurements of varying pH solutions emerging from the molecule, not the superstructure that results from the self-assembly (Fig. S16(c), ESI†).

Cytotoxicity assay

The cytotoxicity of the synthesized **NDI–TA** and NDI was studied *in vitro* using MTT protocol in MDA-MB 231 (Human mammary gland adenocarcinoma cell line) cancerous cells and non-cancerous cells, such as HEK 293 (Human embryonic kidney epithelial cells) with different concentrations.[50,53] The observed results showed that with 50 μg/100 μL **NDI–TA** concentration, more than 80% cell viability was noted, as shown in Fig. 8. Interestingly, '**NDI–TA**' has demonstrated considerable bio-compatibility, but dose-dependent cytotoxicity has been seen at elevated levels compared to NDI.

Cell uptake and morphological investigations

The **NDI–TA** and NDI were treated to MDA-MB 231 (adenocarcinoma cells) at 10 μg/100 μl concentration. The cellular uptake and effect on the cellular morphology were observed using a fluorescence confocal microscope at 60× magnification (Fig. 9). The confocal imaging confirmed the bio-compatibility of **NDI–TA** and NDI in the cells. **NDI–TA** and NDI both were found to be localized in the cell efficiently even at such low treatment concentration. Due to the enhanced solubility of NDI compared to our previous work, NDI here in the cells showed enhanced fluorescence and uptake.[45] Also, we observed a slight dullness in the green fluorescence at identical laser settings for **NDI–TA** when compared to its blue fluorescence. Even at 24 h time points, the fluorescence from NDI and **NDI–TA** were found to be stable (Fig. 9). From these observations, the bio-compatible nature and the fluorescent ability of **NDI–TA** and NDI as ''cellular markers'' and ''delivery agents'' for future studies can be clearly stated.

Conclusions

Herein, we demonstrated that a novel bolaamphiphile, consisting of a naphthalenediimide core and tartaric acid as the head group, was designed and successfully synthesized. By changing pH from 7 to 2 and 7 to 9, **NDI–TA** exhibits the AIEE phenomenon. **NDI–TA** bearing tartaric acid head group exhibits different types of self-assembled aggregates, ranging from cubic or truncated cubic structures and fractal grass-like microstructures. Moreover, the biocompatibility and cellular uptake studies of the **NDI–TA** bolaamphiphile have revealed improved solubility after functionalization and non-toxic nature even at higher concentration in the cells. Interestingly, it has a distinct bluish-green fluorescence that suggests that the **NDI–TA**'s surface functionality may be explored as a cell marker and delivery expedient for real-world applications.

Conflicts of interest

The authors declare that there are no conflicts to declare.

Acknowledgements

S. V. B. (IICT) is grateful for financial support from the DAE-BRNS under the project no. 58/14/01/2020-BRNS/37047, and IICT/Pubs./2020/339. S. M. W. acknowledges CSIR for a senior research fellowship (SRF). M. D. A. is thankful to Umma Al-Qura University for a Scholarship. S. V. B. (GU) acknowledges financial support and a Professorship from the UGC-FRP. N. Puvvada acknowledges the DST-Inspire faculty scheme for financial support. Keerti Bhamidipati acknowledges ICMR for a senior research fellowship (SRF). The authors thank Dr L. Giribabu for TCSPC measurements. This work is dedicated to the late Dr Nilesh L. Patil, one of the finest chemistry students of the School of Chemical Sciences, K. B. C. North Maharashtra University, Jalgaon, Maharashtra, India.

Notes and references

1 J.-H. Fuhrhop and T. Wang, *Chem. Rev.*, 2004, **104**, 2901.
2 R. C. Claussen, B. M. Rabatic and S. I. Stupp, *J. Am. Chem. Soc.*, 2003, **125**, 12680.
3 P. Dhasaiyan and B. L. V. Prasad, *Chem. Rec.*, 2017, **17**, 597.
4 J.-M. Lehn, *Supramolecular Chemistry: Concepts and perspectives*, VCH, Weinheim, 1995, p. 271, softcover, DM 58.00, ISBN 3-527-2931 1996, 8(10).
5 A. S. Mahadevi and G. N. Sastry, *Chem. Rev.*, 2016, **116**, 2775.
6 H. Lodish, A. Berk, S. L. Zipursky, P. Matsudaira, D. Baltimore and J. Darnell, *Molecular Cell Biology*, W. H. Freeman, New York, 4th edn, 2000.
7 E. Frieden, *J. Chem. Educ.*, 1975, **52**, 754.
8 R. Barker, *Organic Chemistry of Biological Compounds*, Prentice-Hall, Englewood Cliffs, New Jersey, 1971.
9 E. Moulin, L. Faour, C. C. Carmona-Vargas and N. Giuseppone, *Adv. Mater.*, 2020, **32**, 1906036.

Published on 26 April 2021. Downloaded by Goa University on 5/3/2021 8:22:12 AM.

10 K. Ariga, M. Nishikawa, T. Mori, J. Takeya, L. K. Shrestha and J. P. Hill, *Sci. Technol. Adv. Mater.*, 2019, **20**, 51.
11 (*a*) M. A. Stuart, W. T. Huck, J. Genzer, M. Müller, C. Ober, M. Stamm, G. B. Sukhorukov, I. Szleifer, V. V. Tsukruk and M. Urban, *et al.*, *Nat. Mater.*, 2010, **9**, 101; (*b*) K. Saha, S. T. Kim, B. Yan, O. R. Miranda, F. S. Alfonso, D. Shlosman and V. M. Rotello, *Small*, 2013, **9**, 300–305.
12 (*a*) J. K. Chen and C. J. Chang, *Materials*, 2014, **7**, 805; (*b*) M. Ding, L. Jing, H. Yang, C. E. Machnicki, X. Fu, K. Li, I. Y. Wong and P. Y. Chen, *Mater. Today Adv.*, 2020, **8**, 100088; (*c*) J. Brinkmann, E. Cavatorta, S. Sankaran, B. Schmidt, J. van Weerd and P. Jonkheijm, *Chem. Soc. Rev.*, 2014, **43**, 4449–4469.
13 T. Han, X. Wang, D. Wang and B. Z. Tang, *Top. Curr. Chem.*, 2021, **7**, 379.
14 S. Ray, A. K. Das and A. Banerjee, *Chem. Mater.*, 2007, **19**, 1633.
15 T. Shimizu, M. Masuda and H. Minamikawa, *Chem. Rev.*, 2005, **105**, 1401.
16 J. Baillet, A. Gaubert, D. M. Bassani, J. Verget, L. Latxague and P. Barthélémy, *Chem. Commun.*, 2020, **56**, 3397.
17 X. Cheng, H. Gao, X. Tan, X. Yang, M. Prehm, H. Ebert and C. Tschierske, *Chem. Sci.*, 2013, **4**, 3317.
18 M. Ikeda, *Polym. J.*, 2019, **51**, 371.
19 Y. Jin, Y. Xia, S. Wang, L. Yan, Y. Zhou, J. Fan and B. Song, *Soft Matter*, 2015, **11**, 798.
20 Y. Sheng, Q. Chen, J. Yao, Y. Wang and H. Liu, *Sci. Rep.*, 2015, **5**, 7791.
21 H. Zhang, J. Shen, Z. Liu, A. Hao, Y. Bai and W. An, *Supramol. Chem.*, 2010, **22**, 297.
22 N. Nuraje, H. Bai and K. Su, *Prog. Polym. Sci.*, 2013, **38**, 302.
23 M. Fariya, A. Jain, V. Dhawan, S. Shah and M. S. Nagarsenker, *Adv. Pharm. Bull.*, 2014, **4**, 483.
24 (*a*) E. I. P. Delbeke, J. Everaert, O. Lozach, T. Le Gall, M. Berchel, T. Montier, P.-A. Jaffrès, P. Rigole, T. Coenye and M. Brennich, *et al.*, *ACS Sustainable Chem. Eng.*, 2018, **6**, 8992; (*b*) Rashmi, A. K. Singh, K. Achazi, B. Schade, C. Böttcher, R. Haag and S. K. Sharma, *RSC Adv.*, 2018, **8**, 31777.
25 (*a*) Q. Xia, Z. Chen, Z. Yu, L. Wang, J. Qu and R. Liu, *ACS Appl. Mater. Interfaces*, 2018, **10**, 17081–17088; (*b*) G. Chen, Y. Yang, Q. Xu, M. Ling, H. Lin, W. Ma, R. Sun, Y. Xu, X. Liu, N. Li, Z. Yu and M. Yu, *Nano Lett.*, 2020, **20**, 8141–8150; (*c*) Y. Yang, Y. Yu, H. Chen, X. Meng, W. Ma, M. Yu, Z. Li and C. Li, *ACS Nano*, 2020, **14**, 13536–13547; (*d*) P. Wu, X. Wang, Z. Wang, W. Ma, J. Guo and J. Chen, *ACS Appl. Mater. Interfaces*, 2019, **11**, 18691–18700.
26 W. Bu, H. Gao, X. Tan, X. Dong, X. Cheng, M. Prehm and C. A. Tschierske, *Chem. Commun.*, 2013, **49**, 1756.
27 G. Wu, P. Verwilst, K. Liu, M. Smet, C. F. J. Faul and X. Zhang, *Chem. Sci.*, 2013, **4**, 4486.
28 S. Schmid, D. Y. W. Ng, E. Mena-Osteritz, Y. Wu, T. Weil and P. Bäuerle, *Chem. Commun.*, 2016, **52**, 3235.
29 N. Bäumer, K. K. Kartha, J. P. Palakkal and G. Fernández, *Soft Matter*, 2020, **16**, 6834.
30 Y. Xiao, R. Zhang, H. Gao, H. Zhao and X. Cheng, *J. Mater. Chem. C*, 2019, **7**, 1237.
31 S. Roy, D. Samanta, P. Kumar and T. K. Maji, *Chem. Commun.*, 2018, **54**, 275.
32 F. Würthner, C. R. Saha-Möller, B. Fimmel, S. Ogi, P. Leowanawat and D. Schmidt, *Chem. Rev.*, 2016, **116**, 962.
33 T. W. Anderson, J. K. M. Sanders and G. D. Pantoş, *Org. Biomol. Chem.*, 2010, **8**, 4274.
34 M. Al Kobaisi, S. V. Bhosale, K. Latham, A. M. Raynor and S. V. Bhosale, *Chem. Rev.*, 2016, **116**, 11685.
35 H. Shao, J. Seifert, N. C. Romano, M. Gao, J. J. Helmus, C. P. Jaroniec, D. A. Modarelli and J. R. Parquette, *Angew. Chem., Int. Ed.*, 2010, **49**, 7688.
36 G. D. Pantoş, P. Pengo and J. K. M. Sanders, *Angew. Chem., Int. Ed.*, 2007, **46**, 194.
37 W. Liyanage, P. W. Rubeo and B. L. Nilsson, *Interface Focus*, 2017, **7**, 20160099.
38 (*a*) S. Basak, N. Nandi, S. Paul and A. Banerjee, *ACS Omega*, 2018, **3**, 2174; (*b*) B. Pramanik and D. Das, *J. Phys. Chem. C*, 2018, **122**, 3655–3661.
39 (*a*) M. B. Avinash and T. Govindaraju, *Acc. Chem. Res.*, 2018, **51**, 414; (*b*) P. Choudhury, S. Sarkar and P. K. Das, *Langmuir*, 2018, **34**(47), 14328–14341; (*c*) D. Chakraborty, D. Sarkar, A. K. Ghosh and P. K. Das, *Soft Matter*, 2021, **17**, 2170–2180.
40 (*a*) M. Kumar and S. J. George, *Nanoscale*, 2011, **3**, 2130; (*b*) P. Choudhury, K. Das and P. K. Das, *Langmuir*, 2017, **33**, 4500–4510.
41 (*a*) S. Goskulwad, D. D. La, M. A. Kobaisi, S. V. Bhosale, V. Bansal, A. Vinu, K. Ariga and S. V. Bhosale, *Sci. Rep.*, 2018, **8**, 11220; (*b*) R. Kumar, S. N. Ugale, A. M. Kale, R. S. Bhosale and R. Narayan, *ChemistrySelect*, 2018, **3**, 9393–9401.
42 S. K. Batabyal, W. L. Leong and J. J. Vittal, *Langmuir*, 2010, **26**, 7464.
43 D. S. Abdelhamid, Y. Zhang, D. R. Lewis, P. V. Moghe, W. J. Welsh and K. E. Uhrich, *Biomaterials*, 2015, **53**, 32.
44 A. Faig, T. D. Arthur, P. O. Fitzgerald, M. Chikindas, E. Mintzer and K. E. Uhrich, *Langmuir*, 2015, **31**, 11875.
45 S. M. Wagalgave, S. D. Padghan, M. Al Kobaisi, D. D. La, K. Bhamidipati, N. Puvvada, R. S. Bhosale, S. V. Bhosale and S. V. Bhosale, *New J. Chem.*, 2020, **44**, 18092.
46 S. P. Goskulwad, M. A. Kobaisi, D. D. La, R. S. Bhosale, M. Ratanlal, S. V. Bhosale and S. V. Bhosale, *Chem. – Asian J.*, 2018, **13**, 3947.
47 (*a*) M. Pandeeswar, M. B. Avinash and T. Govindaraju, *Chem. – Eur. J.*, 2012, **18**, 4818; (*b*) F. Salerno, J. A. Berrocal, A. T. Haedler, F. Zinna, E. W. Meijer and L. D. Bari, *J. Mater. Chem. C*, 2017, **5**, 3609.
48 K. Palo, L. Brand, C. Eggeling, S. Jäger, P. Kask and K. Gall, *Biophys. J.*, 2002, **83**, 605–618.
49 (*a*) A. Sikder, J. Sarkar, R. Barman and S. Ghosh, *J. Phys. Chem. B*, 2019, **123**, 7169; (*b*) Z. Li, Y. Xu, H. Xu, M. Cui, T. Liu, X. Ren, J. Sun, D. Deng, Y. Gu and P. Wang, *Spectrochim. Acta, Part A*, 2021, **244**, 118819.
50 J. Zhao, H. Yang, J. Li, Y. Wang and X. Wang, *Sci. Rep.*, 2017, **7**, 18014.
51 M. J. Frisch, G. W. Trucks, H. B. Schlegel, G. E. Scuseria, M. A. Robb, J. R. Cheeseman, G. Scalmani, V. Barone, G. A. Petersson, H. Nakatsuji, X. Li, M. Caricato,

 This journal is © The Royal Society of Chemistry and the Centre National de la Recherche Scientifique 2021

A. V. Marenich, J. Bloino, B. G. Janesko, R. Gomperts, B. Mennucci, H. P. Hratchian, J. V. Ortiz, A. F. Izmaylov, J. L. Sonnenberg, D. Williams-Young, F. Ding, F. Lipparini, F. Egidi, J. Goings, B. Peng, A. Petrone, T. Henderson, D. Ranasinghe, V. G. Zakrzewski, J. Gao, N. Rega, G. Zheng, W. Liang, M. Hada, M. Ehara, K. Toyota, R. Fukuda, J. Hasegawa, M. Ishida, T. Nakajima, Y. Honda, O. Kitao, H. Nakai, T. Vreven, K. Throssell, J. A. Montgomery, Jr., J. E. Peralta, F. Ogliaro, M. J. Bearpark, J. J. Heyd, E. N. Brothers, K. N. Kudin, V. N. Staroverov, T. A. Keith, R. Kobayashi, J. Normand, K. Raghavachari, A. P. Rendell, J. C. Burant, S. S. Iyengar, J. Tomasi, M. Cossi, J. M. Millam, M. Klene, C. Adamo, R. Cammi, J. W. Ochterski, R. L. Martin, K. Morokuma, O. Farkas, J. B. Foresman and D. J. Fox, *Gaussian 16*, Gaussian Inc., Wallingford CT, 2016.

52 N. M. O'Boyle, A. L. Tenderholt and K. M. Langner, *J. Comput. Chem.*, 2008, **29**, 839.

53 P. Mukherjee, A. Kumar, K. Bhamidipati, N. Puvvada and S. K. Sahu, *ACS Appl. Bio Mater.*, 2020, **3**, 869.

Published on 26 April 2021. Downloaded by Goa University on 5/3/2021 8:22:12 AM.